

Article

Structure–Activity Relationship of Xanthenes as Inhibitors of Xanthine Oxidase

Ling-Yun Zhou ^{1,2}, Jia-Le Peng ³, Jun-Ming Wang ¹, Yuan-Yuan Geng ¹, Zhi-Li Zuo ^{3,*} and Yan Hua ^{1,*}

¹ Key Laboratory for Forest Resources Conservation and Use in the Southwest Mountains of China (Southwest Forestry University), Ministry of Education, Kunming 650224, China; zly4321@sina.com (L.-Y.Z.); dawn723@163.com (J.-M.W.); gyy18254369476@163.com (Y.-Y.G.)

² Anhui Provincial Engineering Research Center for Polysaccharide Drugs, School of Pharmacy, Wannan Medical College, Wuhu 241002, China

³ State Key Laboratory of Phytochemistry and Plant Resource in West China, Kunming Institute of Botany, Chinese Academy of Sciences, Kunming 650201, China; JialePeng2016@163.com

* Correspondence: zuozhili@mail.kib.ac.cn (Z.-L.Z.); huayan1216@163.com (Y.H.); Tel: +86-183-1398-2055 (Z.-L.Z.); +86-138-8866-8877 (Y.H.)

Received: 31 December 2017; Accepted: 7 February 2018; Published: 9 February 2018

Abstract: Polygala plants contain a large number of xanthenes with good physiological activities. In our previous work, 18 xanthenes were isolated from *Polygala crotalarioides*. Extended study of the chemical composition of the other species *Polygala sibirica* led to the separation of two new xanthenes—3-hydroxy-1,2,6,7,8-pentamethoxy xanthone (A) and 6-O-β-D-glucopyranosyl-1,7-dimethoxy xanthone (C)—together with 14 known xanthenes. Among them, some xanthenes have a certain xanthine oxidase (XO) inhibitory activity. Furthermore, 14 xanthenes as XO inhibitors were selected to develop three-dimensional quantitative structure–activity relationship (3D-QSAR) using comparative molecular field analysis (CoMFA) and comparative molecular similarity indices analysis (CoMSIA) models. The CoMFA model predicted a q^2 value of 0.613 and an r^2 value of 0.997. The best CoMSIA model predicted a q^2 value of 0.608 and an r^2 value of 0.997 based on a combination of steric, electrostatic, and hydrophobic effects. The analysis of the contour maps from each model provided insight into the structural requirements for the development of more active XO inhibitors.

Keywords: xanthone; xanthine oxidase inhibitors; 3D-QSAR; gout

1. Introduction

Xanthenes are a class of natural products commonly occurring in a few higher plant families [1] and have been shown to display a wide range of pharmacological properties [2,3]. An important natural source of these compounds is the Polygalaceae family which includes about 22 genera and 1300 species [4]. In our previous works [5,6], 18 xanthenes were isolated from *Polygala crotalarioides*, some of which have the inhibitory activity against XO. This bioactivity attracted us to investigate more xanthenes from other genus of this family. In the present work, 2 new xanthenes (compounds A and C, Figure 1) and 14 known xanthenes were isolated from *Polygala sibirica* L. var. megalopha Fr. The bioactivity results showed that all 14 tested xanthenes (Figure 2) had a certain inhibition activity against XO. Today, the ligand-based drug design (LBDD) is an important part in computer-aided drug design (CADD) [7,8]. Comparative molecular field analysis (CoMFA) [9] and comparative molecular similarity indices analysis (CoMSIA) [10,11] represent the successful and widely used LBDD approaches for guiding the strategies of chemical derivative modifications [12]. Conventional CoMFA uses electrostatic and steric molecular interaction fields, while CoMSIA includes hydrogen bonding and hydrophobic fields additionally [13,14]. The alignment of molecules was important for

QSAR modeling. Especially, the alignment based on docking was normally more reasonable than on common structures as it takes the binding pose in the receptor into consideration. It also provides us convenience for docking as many crystal structures of XO have been released [15–18]. Herein, we studied the structure–activity relationship (SAR) of xanthenes as inhibitors of XO through 3D-QSAR techniques based on molecular docking. We expect that our work could provide complementary and useful information to discover novel potent XO inhibitors.

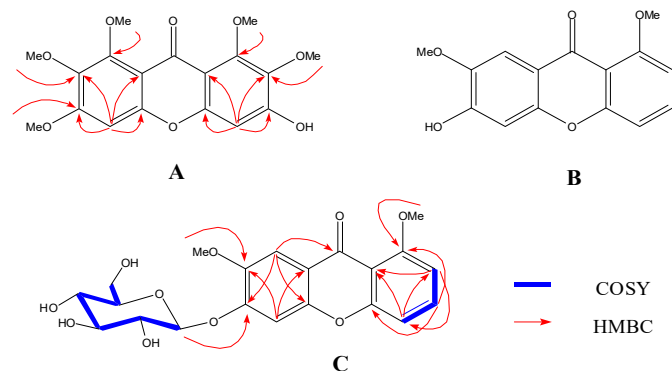


Figure 1. The structure of compounds A–C from *Polygala sibirica*.

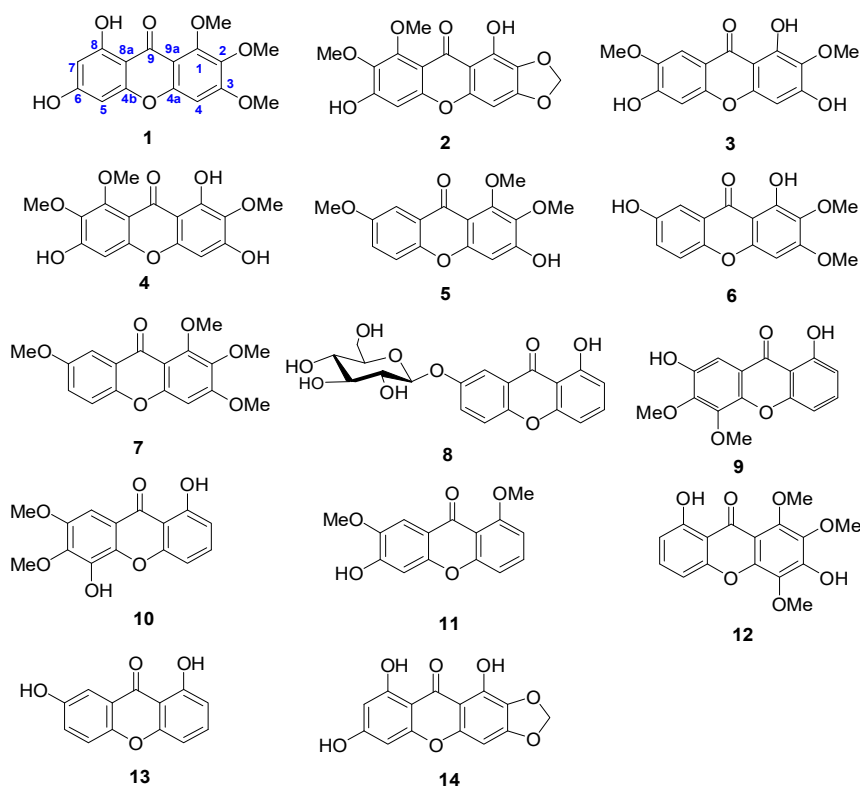


Figure 2. The structure of the 14 xanthenes studied.

2. Results and Discussion

2.1. Identification of New Compounds

Compound A was obtained as a yellow amorphous powder and its molecular formula ($C_{18}H_{18}O_8$) was determined based on the HR-ESI-MS data (m/z 575.1667 [$M + Na$] $^+$ calcd. for 575.1741). The UV spectrum revealed maxima at 208, 245, 277, and 308 nm. The IR exhibited absorption bands at ν_{max}

3425 (O–H), 1611 (chelated C=O), 1510 (aromatic ring) cm^{-1} . Its ^{13}C -NMR spectral data (Table 1) showed the presence of five methoxyl signals, 1 carbonylcarbon signal, as well as 12 aromatic carbons. These spectral data indicated the presence of a hexasubstituted xanthone. The carbon signal at δ_{C} 172.8 is characteristic for a doubly unchelated carbonyl [19] and four of five methoxyl signals (56.6, 60.9, 61.0, 61.7, and 61.8) were typical of di-ortho-substituted methoxyl groups ($\delta_{\text{C}} > 60$) [20]. The ^1H -NMR spectrum of **A** showed two aromatic proton singlets at δ_{H} 6.63 and 6.87, assignable to H-4 and H-5, respectively. The structure of **A** was further confirmed by the HMBC spectrum (Figure 1). On the basis of the above evidence, the structure of **A** was elucidated as 3-hydroxy-1,2,6,7,8-pentamethoxyxanthone.

Table 1. The ^1H (600 MHz) and ^{13}C -NMR (125 MHz) data of **A** in $\text{DMSO-}d_6$.

Position	δ_{H}	δ_{C}
1		153.2 s
2		138.6 s
3		156.6 s
4	6.63 (s)	98.8 d
5	6.87 (s)	96.2 d
6		157.7 s
7		138.9 s
8		152.8 s
9		172.8 s
4a		152.8 s
8a		110.4 s
9a		109.6 s
10a		152.9 s
OMe-1	3.80 (s)	61.7 q
OMe-2	3.74 (s)	61.0 q
OMe-6	3.89 (s)	56.5 q
OMe-7	3.72 (s)	60.9 q
OMe-8	3.81 (s)	61.8 q

Compound **B** was isolated as an amorphous yellow powder. Based on the ESI-MS of **B** indicating $[\text{M} + \text{Na}]^+$ at m/z 311, its molecular formula was deduced to be $\text{C}_{15}\text{H}_{12}\text{O}_5$. The UV spectrum showed absorption maxima at 205, 245, 285, and 358 nm, suggesting the presence of a xanthone skeleton. The ^1H -NMR spectrum of **B** showed the presence of three methoxyl signals at 3.84 and 3.86, two singlets of aromatic protons at 6.84 (s, H-5) and 7.39 (s, H-8) and three mutual coupling signals of aromatic protons. Finally, compound **B** was determined as 6-hydroxy-1,7-dimethoxyxanthone by the comparison of the literature [21].

Compound **C**, amorphous yellow powder, was analyzed for $\text{C}_{21}\text{H}_{22}\text{O}_{10}$ by HR-ESI-MS at m/z 457.1110 $[\text{M} + \text{Na}]^+$ (calcd. for 457.1105). The ^1H -NMR and ^{13}C -NMR spectra of **C** (Table 2) were similar to those of **B**, except that signals corresponding to the sugar moiety included an anomeric proton signal ($\delta = 5.88$ (1H, d, $J = 7.5$ Hz)) and anomeric carbon signal ($\delta = 101.6$). On acid hydrolysis, **C** gave a D-glucose unit by comparison with the authentic sample on GC. The relative configuration of the glucose residue was deduced to be β by the coupling constants (J) of 7.5 Hz. In the HMBC spectrum, the glucosyl group was propamorphous yellow powdered at C-6 by the correlations from Glc-H-1 (δ_{H} 5.88, $J = 7.5$ Hz) to C-6 (δ_{C} 153.2). Furthermore, the structure of compound **C** was further confirmed by the HMBC and ^1H - ^1H COSY spectrum. Therefore, the structure of **C** was formulated as 6-O- β -D-glucopyranosyl-1,7-dimethoxyxanthone.

Table 2. The ^1H (600 MHz) and ^{13}C -NMR (125 MHz) data of **C** in $\text{DMSO-}d_5$.

Position	δ_{H}	δ_{C}
1		160.8 s
2	6.97 (d, 8.2)	110.0 d
3	7.51 (t, 8.2)	134.4 d
4	6.76 (d, 8.2)	105.9 d
5	7.59 (s)	103.8 d
6		153.2 s
7		147.3 s
8	7.89 (s)	106.6 d
9		174.7 s
4a		158.3 s
8a		117.2 s
9a		112.5 s
10a		150.8 s
OMe-1	3.83 (s)	56.1 q
OMe-7	3.67 (s)	55.7 q
Glc-1	5.88 (d, 7.5)	101.6 d
2	4.42 (m)	74.5 d
3	4.44 (m)	78.3 d
4	4.40 (m)	70.9 d
5	4.35 (m)	79.2 d
6	4.57 (d, 11.7) 4.40 (m)	62.2 t

2.2. CoMFA and CoMSIA Analysis

Table 3 showed the predicted pIC_{50} values for 14 xanthenes (Figure 2), and the differences between the predicted and experimental pIC_{50} values are given as well. The CoMFA model was obtained using the training set of 14 xanthenes, and all corresponding statistical parameters were listed in Table 4. Figure 3 showed the relationship between the CoMFA

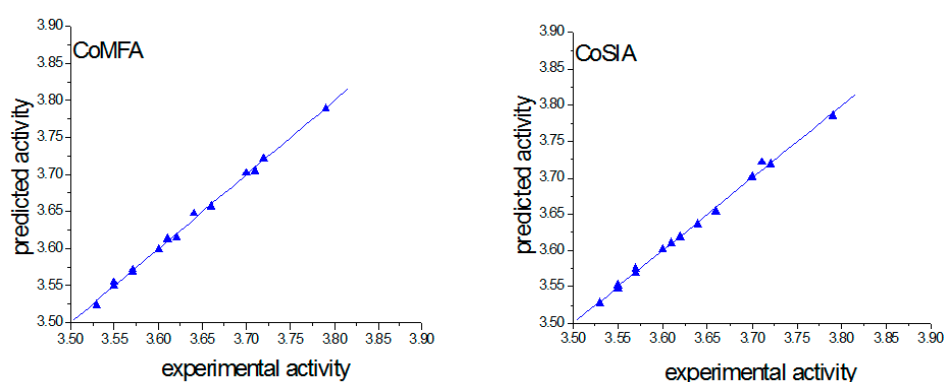
Table 3. Xanthenes and their observed and predicted (pre.) XO inhibition activities.

Number	pIC_{50}	CoMFA		CoMSIA	
		pre. pIC_{50}	Residue	pre. pIC_{50}	Residue
1	3.66	3.657	−0.003	3.654	−0.006
2	3.64	3.648	0.008	3.636	−0.004
3	3.79	3.789	−0.001	3.785	−0.005
4	3.71	3.705	−0.005	3.721	0.011
5	3.55	3.551	0.001	3.547	−0.003
6	3.60	3.599	−0.001	3.601	0.001
7	3.62	3.615	−0.005	3.619	−0.001
8	3.72	3.722	0.002	3.719	−0.001
9	3.57	3.569	−0.001	3.57	0
10	3.57	3.572	0.002	3.575	0.005
11	3.55	3.555	0.005	3.553	0.003
12	3.61	3.613	0.003	3.61	0
13	3.53	3.524	−0.006	3.528	−0.002
14	3.70	3.702	0.002	3.701	0.001

Predicted and experimental pIC_{50} values, from which it can be seen that all points are located near the diagonal line. The high q^2 , r^2 and F -values, along with the low SEE value, indicated a good statistical correlation and reasonable predictability of the CoMFA model. The best CoMSIA model was developed using three descriptor fields: steric, electrostatic and hydrophobic fields. According to the CoMFA analysis method, a good statistical correlation, and reasonable predictability of the CoMSIA model were also indicated from Table 4 and Figure 3.

Table 4. Statistical parameters of CoMFA and CoMSIA model.

Method	CoMFA	CoMSIA
<i>PLS statistics</i>		
q^2	0.613	0.608
SEP	0.065	0.066
Optimum components	6	6
r^2	0.997	0.997
SEE	0.005	0.006
F-ratio	426	0.997
<i>Field distribution</i>		
Steric	0.632	0.152
Electrostatic	0.368	0.316
Hydrophobic		0.532

**Figure 3.** Plot of experimental against predicted pIC_{50} by CoMFA and CoMSIA.

2.3. Verification of Model Reliability

Using the established model, we predicted the relative values of all 14 xanthenes and sorted their values. From the order of the original activity, the prediction of the model and the order of docking scoring (Table 5), it was found that the order of activity of Compounds **4**, **8**, and **14** with relatively high activity was relatively in front, and compound **13** with the ranking of the lowest active was still backward, and the order of the predicted value was basically the same as that of the original activity. The results showed that the activity value predicted by the model is reliable.

Table 5. The relative experimental and predicted (pre.) values order of 14 xanthenes.

Number	pIC_{50}	coMFA-pre. pIC_{50}	coMSIA-pre. pIC_{50}	Original Activity Order	CoMFA pre. Activity Order	CoMSIA pre. Activity Order	Docking Score	Docking Score Order
1	3.66	3.657	3.654	3	8	4	72.23	2
2	3.64	3.648	3.636	8	4	8	71.41	8
3	3.79	3.789	3.785	4	14	14	60.48	9
4	3.71	3.705	3.721	14	2	2	60.59	14
5	3.55	3.551	3.547	1	3	3	53.7	4
6	3.6	3.599	3.601	2	7	7	54.48	3
7	3.62	3.615	3.619	7	12	12	45.98	6
8	3.72	3.722	3.719	12	6	6	64.35	10
9	3.57	3.569	3.570	6	10	1	62.93	5
10	3.57	3.572	3.575	9	9	10	54.32	1
11	3.55	3.555	3.553	10	11	9	50.12	11
12	3.61	3.613	3.610	5	5	11	49.86	12
13	3.53	3.524	3.528	11	1	5	38.95	7
14	3.7	3.702	3.701	13	13	13	61.05	13

2.4. CoMFA and CoMSIA Contour Maps

Contour maps of CoMFA and CoMSIA (Figures 4 and 5) gave a semi-quantitative information for the structure of all 14 xanthenes. Compound 3 was used as the reference molecule. The green contours represent regions where bulky substituents would increase the activity, while the yellow contours represent regions where the steric bulky group would be unfavorable. Furthermore, the blue and red contours depict the position where positively charged groups and negatively charged groups would be favorable, respectively. In addition, the purple and orange regions represent the effect of the electrostatic field on the activity of the compounds. The introduction of hydrophobic groups in the purple region can improve the activity of the compound, and the introduction of the hydrophilic group in the orange region is beneficial to the activity.

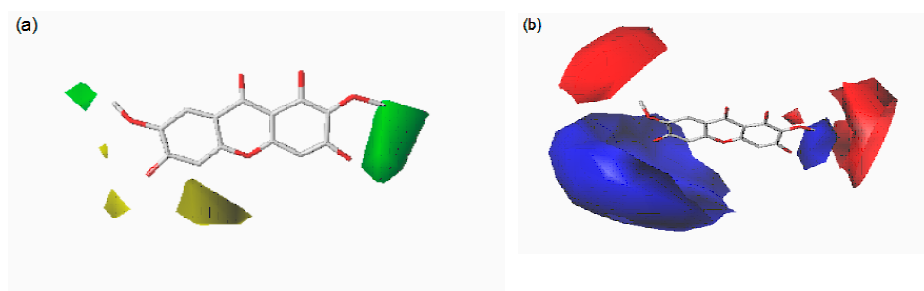


Figure 4. Contour maps of CoMFA: steric (a) and electrostatic (b) based on Compound 3.

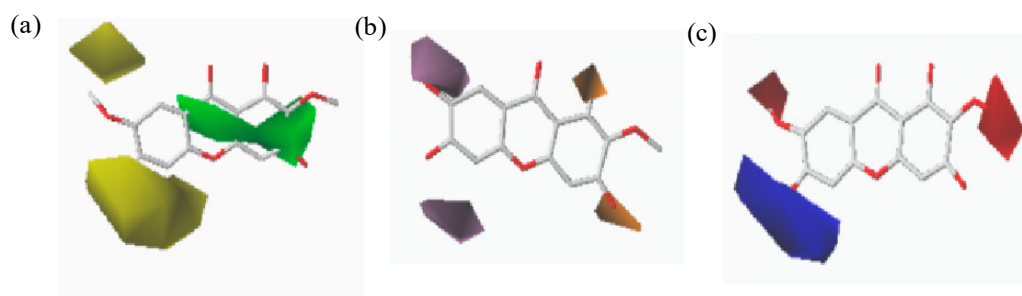


Figure 5. Contour maps of CoMSIA: steric (a); electrostatic (b); and hydrophobic (c) based on Compound 3.

Compound 3 has the highest activity value, and its various maps are representative. However, because the molecular docking is not as regular as the skeleton overlap, the situation of each molecule placed into the active cavity docking is different. In order to analyze comprehensively, each molecule would be placed in the three-dimensional field, electrostatic field, and hydrophobic field.

As shown in Figure 6, each molecule was placed in a steric field and analyzed in detail. It was found that the yellow region tended to be close to the 1, 8 position of the compound, indicating that the two positions should be not suitable for introduction of groups. This may be the reason why Compound 3 with no substitutions at 8-position was more potent than Compound 4 with a methoxy substituent. The green region tended to approach the 2-, 3-, 6-, and 7-position of the compound, indicating that these positions may be suitably introduced into the group and that the larger groups may favor the activity increase, which explain why Compound 13 without the glycosyl group at 7-position had weak activity compared to Compound 8 with a glycosyl substitution. The 4,5-position information of the compound was not obvious.

As shown in Figure 7, each molecule was placed in an electrostatic field and analyzed in detail. It was found that the blue region tended to be close to the 1, 8 position of the compound, indicating that the introduction of positively charged groups at this site should increase the activity. Compound 3 with

no substituent at the 8-position had better activity compared to Compound 4 being oxygen-substituted. This also confirmed the previous inference that its 1- and 8-position should be no substituent. The red region tended to be close to the 7-position of the compound, indicating that the introduction of a negatively charged group can increase the activity of the compound.

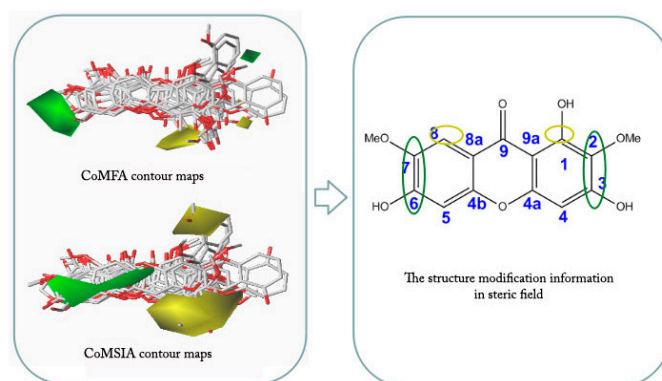


Figure 6. Steric field views of 14 xanthenes.

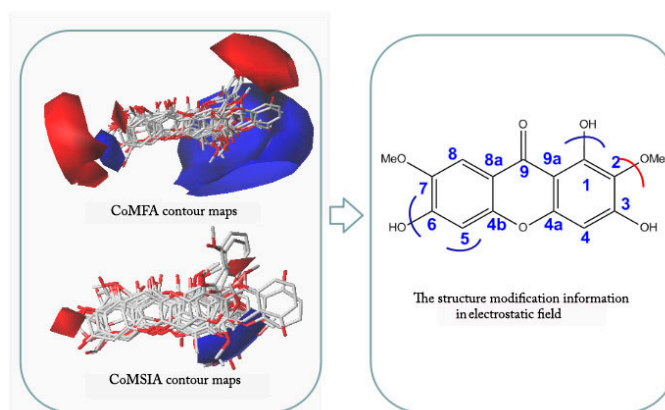


Figure 7. Electrostatic field views of 14 xanthenes.

The incorporation of a hydrophilic group at the 2, 3, 6, 7 position of the compound (as shown in the orange region of Figure 8) should enhance the activity while the purple region tended to be close to 1, 4, indicating the introduction of hydrophobicity at both positions groups were conducive to increasing the activity.

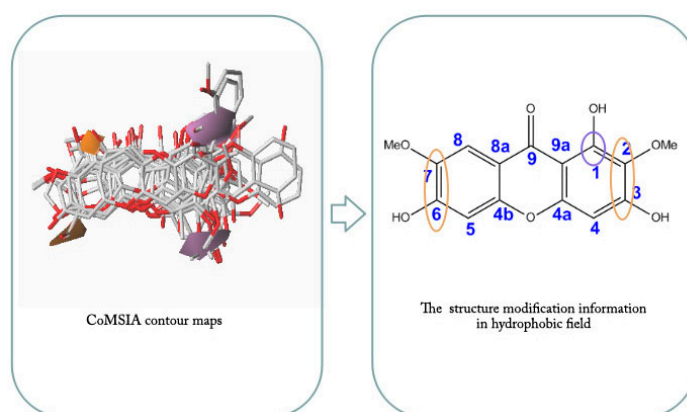


Figure 8. Hydrophobic field views of 14 xanthenes.

3. Experimental Section

3.1. General Information

Optical rotations were recorded using a P-1020 digital polarimeter (Jasco, Tokyo, Japan). The UV spectra were measured on a UV-2401PC spectrophotometer (Shimadzu, Suzhou, China). The IR spectra were recorded as KBr pellets on a Tensor-27 spectrometer (Bruker, Bremen, Germany). The NMR spectra were recorded on an AM-400 spectrometer (Bruker) with TMS as an internal standard. ESI-MS and HR-EI-MS-TOF-MS were measured on a Bruker HTC/Esquire spectrometer and a Bruker Daltonics Flex spectrometer, respectively. GC analysis was carried out on an HP-5890 II system (Gentech Scientific, Alto, CA, USA) equipped with a FID detector and a HP-20M capillary column (25 m × 0.32 mm × 0.3 μm). Column chromatography was performed with silica gel (Qingdao Marine Chemical Industry Factory, Qingdao, China) and Sephadex LH-20 (GE Healthcare Bio-Sciences AB, Fairfield, CT, USA) and reversed-phase C18 silica gel (40–60 μm, Merck, Darmstadt, Germany). TLC was performed with silica gel GF254 (Qingdao Marine Chemical Industry Factory). Fractions were monitored by TLC and spots were visualized by heating after spraying with 5% H₂SO₄ in ethanol.

3.2. Plant Material

The whole plant of *P. Sibirica* L. Var megalopha Fr. were collected in Yongshan, Yunnan Province, People's Republic of China. A voucher specimen (HUA002) was identified by Prof. Fan Du (Southwest Forestry University) and was deposited at the College of Forestry, Southwest Forestry University.

3.3. Extraction, Isolation, and Characterization

The 75% ethanol extract of the whole dry plant of *Polygala sibirica* (5.0 kg) was purified using chromatography with D101 macroporous resin and the column contents were eluted with H₂O, 35% EtOH, 65% EtOH, and 95% EtOH, using a gradient. The 65% EtOH elute was concentrated in vacuo to afford a residue (480 g), which was subjected to silica gel column chromatography, using a CHCl₃–MeOH gradient (50:1→0:1) as the eluent to separate it into 13 fractions (Fr1–Fr13). Fr2 (8 g) was applied to MCI-gel column with MeOH–H₂O gradient (1:1→1:0) to afford four fractions (Fr2A–Fr2D). Fr2B (1.9 g) was chromatographed on a silica gel column and eluted in a step gradient manner with a CHCl₃:MeOH (15:1→0:1) gradient system to afford five fractions 2B1–2B5. Subfraction 2B2 (0.9 g) was further purified by Sephadex LH-20 (CHCl₃:MeOH = 1:1) chromatography and semi-prepared HPLC (CH₃CN:H₂O = 40:60, λ = 254 nm) to produce compound **A** (retention time = 11.5 min, 5.6 mg) and compound **B** (retention time = 8.2 min, 10.4 mg). Subfraction 2B5 (0.5 g) was further purified by Sephadex LH-20 (CHCl₃:MeOH = 1:1) chromatography and semi-prepared HPLC (CH₃CN:H₂O = 30:70, λ = 254 nm, retention time = 14.1 min) to produce compound **C** (8.6 mg). 3-hydroxy-1,2,6,7,8-pentamethoxyxanthone (**A**): yellow amorphous powder; HR-ESI-MS *m/z*: 385.0899 [M + Na]⁺ (calcd. for 385.0894, C₁₈H₁₈O₈Na⁺); [α]_D²⁰ –22.59° (c 0.9, MeOH); UV (CH₃OH) λ_{max} (log ε): 308 (4.29), 277 (4.07), 245 (4.62), 208 (4.46); IR (KBr) ν_{max}: 3425, 2936, 2853, 1611, 1510, 1468, 1424, 1384, 1273, 1123, 1080, 1061, 993 cm⁻¹; ¹H-NMR and ¹³C-NMR data see Table 1.

6-Hydroxy-1,7-Dimethoxyxanthone (**B**): yellow amorphous powder; ESI-MS *m/z*: 317 [M + K]⁺, 311 [M + Na]⁺ and 289 [M + H]⁺; UV (CH₃OH) λ_{max} (log ε): 358 (4.022), 285 (3.987), 245 (4.186), 205 (4.517); ¹H-NMR (400 MHz, DMSO-*d*₆) δ: 7.62 (1H, t, *J* = 8.5 Hz, H-3), 7.39 (1H, s, H-8), 7.04 (1H, d, *J* = 7.8 Hz, H-4), 6.90 (1H, d, *J* = 8.2 Hz, H-2), 6.84 (1H, s, H-5), 3.86 (3H, s, OMe-1), 3.84 (3H, s, OMe-7); ¹³C-NMR (100 MHz, DMSO-*d*₆) δ: 160.0 (s, C-1), 106.1 (d, C-2), 134.4 (d, C-3), 109.5 (d, C-4), 102.3 (d, C-5), 153.8 (s, C-6), 146.0 (s, C-7), 105.6 (d, C-8), 173.6 (s, C-9), 157.4 (s, C-4a), 114.4 (s, C-8a), 111.3 (s, C-9a), 150.5 (s, C-10a), 56.1 (q, OMe-1), 56.8 (q, OMe-7).

6-O-β-D-Glucopyranosyl-1,7-Dimethoxyxanthone (**C**): yellow amorphous powder; HR-ESI-MS *m/z*: 457.1110 [M + Na]⁺ (calcd. for 457.1105, C₂₁H₂₂O₁₀Na⁺); [α]_D²⁰ –112.78° (c 0.8, MeOH); UV (CH₃OH)

λ_{\max} (log ϵ): 360 (4.137), 283 (4.215), 247 (4.586), 203 (4.717); IR (KBr) ν_{\max} : 3417, 2925, 1620, 1503, 1476, 1433, 1385, 1270, 1177, 1077, 806, 583 cm^{-1} ; $^1\text{H-NMR}$ and $^{13}\text{C-NMR}$ data, see Table 2.

3.4. Acid Hydrolysis of Compound C

A solution of **C** (3 mg) in 1 M HCl (3 mL) was heated in a water bath at 70 °C for 6 h. After cooling, the reaction mixture was neutralized with NaHCO_3 and extracted with CHCl_3 . The aqueous solution was further concentrated to dryness and dissolved in 1 mL pyridine. Then hydroxyl-ammonium hydrochloride (1 mg) was added. The solution were kept in a 80 °C water bath for 30 min, followed by treatment with 1 mL Ac_2O and kept in a 90 °C water bath for another 40 min. The authentic monosaccharide samples were treated similarly as the hydrolysis products. Finally, 1 μL of these acetylated sugars were injected into a HP-20M capillary column using N_2 as carrier (oven temp. 210 °C) to be analyzed by GC using a FID detector (detector temp. 280 °C). Ultimately, the sugar was determined to be D-glucose by comparing the retention time with that of standard sample: t_R : D-glucose 8.686 min.

3.5. Bioassay of Xanthine Oxidase Inhibitory Activity

The enzyme xanthine oxidase catalyzes the oxidation of xanthine to uric acid. Inhibition of xanthine oxidase results in a decreased production of uric acid. The uric acid production was measured according to the increasing absorbance at 290 nm. Test solutions were prepared by adding xanthine (final concentrations 50 μM), hydroxylamine (final concentration 0.2 mM), EDTA (final concentration 0.1 mM), and flavonol glycosides in four concentrations (2.5, 5.0, 10.0, 20.0 μM). The reaction was started by adding 0.2 mL of xanthine oxidase (6.25 mU/mL) in a phosphate buffer solution (pH = 7.50, 200 mM). The mixture (total 1 mL) was incubated for 30 min at 37 °C. Prior to the measurement of uric acid production, the reaction was stopped by adding 0.1 mL of HCl (0.58 M) [22]. The IC_{50} values were calculated by the mean data values from three determinations.

3.6. Dataset Preparation

All 14 xanthonones and their biological activities were performed by our own. Two-dimensional structures of xanthonones were sketched by Chem-Draw 12.0 software and then converted into three-dimensional structures by GOLD software (Version 3.1, Genetic Optimization of Ligand Docking, London, UK). Correctly re-docking in the protein crystal structure is a key requirement to predict the binding poses. Since the XO protein (PDB entry: 1N5X) was downloaded from the protein data bank [1N5X], it was prepared by removing water and solvent molecules, adding hydrogen atoms, loading charges, and amending amino acid residues. The original molecule TEI-6720 in the protein was extracted as a reference ligand in the docking process to explore the root mean square deviation (RMSD). As a result, the scoring function of CHEMPLP and the docking template of chemscore kinase were selected as this combination afforded a RMSD of 0.506. Therefore, these 14 compounds were docked by the selected docking template and scoring function to obtain the poses which were employed in the QSAR modeling later. Then the activities of all xanthonones along with its pIC_{50} values were transformed and were given in Table 3. The values of pIC_{50} of the dataset set ranging from 3.53 to 3.79 are supposed to contribute to the appropriateness of the training set xanthonones.

3.7. CoMFA and CoMSIA Studies

The 3D-QSAR modelling was carried out in Sybyl-X 2.0 (Tripos, Inc., St. Louis, MO, USA). The CoMFA models were developed on the training set of 14 molecules and validated by the test set of the same molecules, in which Lennard-Jones and Coulomb potentials were employed to calculate the CoMFA steric and electrostatic fields respectively, using the sp^3 carbon as the probe atom having a + 1 charge to determine the magnitude of the field values. The steric and electrostatic energy cutoff was set to 33 kcal/mol with the column-filtering value set to 2.0 kcal/mol. The CoMSIA was similar to

CoMFA about the fields around the aligned molecules, and the other descriptor named hydrophobic effect was calculated together.

3.8. Validation of 3D-QSAR Models

Internal validation was performed using partial least square (PLS) analysis on the training set, in which leave-one-out (LOO) method was used to determine the cross-validated q^2 and the optimal number of components (ONC), and non-cross-validation was performed to calculate conventional r^2 using the same number of components. The external validation (r_{pred}^2) was recommended for the assessment of the predictive abilities of CoMFA and CoMSIA models on the test set. Predictive r_{pred}^2 were calculated as

$$r_{\text{pred}}^2 = 1 - \text{PRESS}/\text{SD} \quad (1)$$

in which SD is the sum of squared deviations between the experimental inhibitory activity of the test set and the mean experimental inhibitory activity of the training set molecules, PRESS is the sum of squared deviations between the predicted and experimental activity values for every molecule in the test set.

4. Conclusions

The chemical constituents of *Polygala sibirica* led to two new xanthenes. Combined with the previously isolated xanthenes from the *Polygala crotalarioides*, we investigated the activity of xanthenes against XO. On the basis of these data, three-dimensional quantitative structure–activity relationships (3D-QSAR) models using CoMFA and CoMSIA were utilized to investigate structural requirements for improving potency of xathone derivatives as XO inhibitors. Authentic CoMFA model ($q^2 = 0.613$, $r^2 = 0.997$) and CoMSIA model ($q^2 = 0.608$, $r^2 = 0.997$) were developed and validated. Analysis of model parameters and contour maps provided details of the structure–activity relationship. We expect this is quite helpful to develop new xathone XO inhibitory lead compounds, which can provide a promising approach to treat gout.

Acknowledgments: The authors are grateful for supports from Yunnan Forest Resources Cultivation and Utilization Collaborative Innovation Center, National Natural Science Foundation of China (no. 31260083), and Wannan Medical College Cultivating Foundation (no. WK2016Z06).

Author Contributions: L.-Y.Z., Z.-L.Z., and Y.H. designed research; L.-Y.Z. and Y.-Y.G. performed the isolation and purification of plants, then analyzed the data; L.-Y.Z., J.-L.P., and J.-M.W. conducted the bioassay of xanthine oxidase inhibitory activity and establish structure–activity relationship; L.-Y.Z. and J.-L.P. wrote the paper. All authors read and approved the final manuscript.

Conflicts of Interest: The authors declare no conflict of interest.

References

1. Cardona, M.L.; Fernández, I.; Pedro, J.R.; Serrano, A. Xanthenes from *Hypericum reflexum*. *Phytochemistry* **1990**, *29*, 3003–3006. [[CrossRef](#)]
2. Peres, V.; Nagem, T.J. Trioxygenated naturally occurring xanthenes. *Phytochemistry* **1996**, *44*, 191–214. [[CrossRef](#)]
3. Peres, V.; Nagem, T.J.; de Oliveira, F.F. Tetraoxygenated naturally occurring xanthenes. *Phytochemistry* **2000**, *55*, 683–710. [[CrossRef](#)]
4. Rocha, J.L.C.; Pastore, J.F.B.; Brandão, H.N.; Azevedo, A.; David, J.P.; Santos, E.O.; David, J.M. Quantificação de salicilato de metila em quatro gêneros de Polygalaceae, por CLAE-DAD. *Quim. Nova* **2012**, *35*, 2263–2266. [[CrossRef](#)]
5. Hua, Y.; Chen, C.X.; Liu, Y.Q.; Chen, S.K.; Zhou, J. Three New Xanthenes from *Polygala crotalarioides*. *Chin. Chem. Lett.* **2006**, *17*, 773–775.
6. Hua, Y.; Chen, C.X.; Liu, Y.Q.; Zhou, J. Two new xanthenes from *Polygala crotalarioides*. *J. Asian Nat. Prod. Res.* **2007**, *9*, 273–275. [[CrossRef](#)] [[PubMed](#)]
7. Shim, J.; Mac Kerell, A.D. Computational ligand-based rational design: Role of conformational sampling and force fields in model development. *Med. Chem. Commun.* **2011**, *2*, 356–370. [[CrossRef](#)] [[PubMed](#)]

8. Richards, W.G. Computers in drug design. *Pure Appl. Chem.* **1993**, *65*, 231–234. [[CrossRef](#)]
9. Cramer, R.D.; Patterson, D.E.; Bunce, J.D. Comparative molecularfield analysis (CoMFA) 1. Effect of shape on binding of steroids to carrier proteins. *J. Am. Chem. Soc.* **1988**, *110*, 5959–5967. [[CrossRef](#)] [[PubMed](#)]
10. Klebe, G.; Abraham, U.; Mietzner, T. Molecular similarity indexes in a comparative-analysis (CoMSIA) of drug molecules to correlate and predict their biological-activity. *J. Med. Chem.* **1994**, *37*, 4130–4146. [[CrossRef](#)] [[PubMed](#)]
11. Klebe, G. Comparative molecular similarity indices analysis: CoMSIA. *Perspect. Drug Discov. Des.* **1998**, *12*, 87–104. [[CrossRef](#)]
12. Verma, J.; Khedkar, V.M.; Coutinho, E.C. 3D-QSAR in drug design: A review. *Curr. Top. Med. Chem.* **2010**, *10*, 95–115. [[CrossRef](#)] [[PubMed](#)]
13. Klebe, G.; Abraham, U. Comparative molecular similarity index Analysis (CoMSIA) to study hydrogen-bonding properties and to score combinatorial libraries. *J. Comput. Aided Mol. Des.* **1999**, *13*, 1–10. [[CrossRef](#)] [[PubMed](#)]
14. Abraham, D.J.; Kellogg, G.E. The effect of physical organic properties on hydrophobic fields. *J. Comput. Aided Mol. Des.* **1994**, *8*, 41–49. [[CrossRef](#)] [[PubMed](#)]
15. Ishikita, H.; Eger, B.T.; Okamoto, K.; Nishino, T.; Pai, E.F. Protein conformational gating of enzymatic activity in xanthine oxidoreductase. *J. Am. Chem. Soc.* **2012**, *134*, 999–1009. [[CrossRef](#)] [[PubMed](#)]
16. Okamoto, K.; Eger, B.T.; Nishino, T.; Kondo, S.; Pai, E.F.; Nishino, T. An Extremely Potent Inhibitor of Xanthine Oxidoreductase Crystal Structure of the Enzyme-Inhibitor Complex and Mechanism of Inhibition. *J. Biol. Chem.* **2003**, *278*, 1848–1855. [[CrossRef](#)] [[PubMed](#)]
17. Enroth, C.; Eger, B.T.; Okamoto, K.; Nishino, T.; Nishino, T.; Pai, E.F. Crystal structures of bovine milk xanthine dehydrogenase and xanthine oxidase: Structure-based mechanism of conversion. *Proc. Natl. Acad. Sci. USA* **2000**, *97*, 10723–10728. [[CrossRef](#)] [[PubMed](#)]
18. Fukunari, A.; Okamoto, K.; Nishino, T.; Eger, B.T.; Pai, E.F.; Kamezawa, M.; Yamada, I.; Kato, N. Y-700 [1-[3-Cyano-4-(2,2-dimethylpropoxy)phenyl]-1H-pyrazole-4-carboxylic acid]: A potent xanthine oxidoreductase inhibitor with hepatic excretion. *J. Pharmacol. Exp. Ther.* **2004**, *311*, 519–528. [[CrossRef](#)] [[PubMed](#)]
19. Van der Sluis, W.G.; Labadie, R.P. Polyoxygenated xanthenes of *Centaurium littorale*. *Phytochemistry* **1985**, *24*, 2601–2605. [[CrossRef](#)]
20. Agrawal, P.K.; Rastogi, R.P. ¹³C-NMR spectroscopy of flavonoids. *Heterocycles* **1981**, *16*, 2181–2236.
21. Hideki, T.; Munekazu, I.; Kohichi, M.; Ito, T.; Tanaka, T.; Chelladurai, V.; Riswan, S. Three xanthenes from *Poeciloneuron pauciflorum* and *Mammea acuminata*. *Phytochemistry* **1997**, *45*, 133–136.
22. Paul, C.; Li, Y.; Mario, C.; Jia, P.H.; Kanyanga, C.; Bart, V.P.; Luc, P.; Arnold, J.V.; Dirk, V.B. Structure–activity relationship and classification of flavonoids as inhibitors of xanthine oxidase and superoxide scavengers. *J. Nat. Prod.* **1998**, *61*, 71–76.

Sample Availability: Samples of the compounds **A** and **B** are not available from the authors because of the limited amount.



© 2018 by the authors. Licensee MDPI, Basel, Switzerland. This article is an open access article distributed under the terms and conditions of the Creative Commons Attribution (CC BY) license (<http://creativecommons.org/licenses/by/4.0/>).